Journal of Materials Chemistry C

Control of aggregation and dissolution of small molecules hole transport layer through a doping strategy of highly efficient perovskite solar cell

Journal:	*Journal of Materials Chemistry C*
Manuscript ID	TC-ART-06-2019-003120.R1
Article Type:	Paper
Date Submitted by the Author:	06-Aug-2019
Complete List of Authors:	Ali, Jazib; Shanghai Jiao Tong University, School of physics Song, Jingnan; Shanghai Jiao Tong University Li, Yu ; Shanghai Jiao Tong University - Minhang Campus, School of Physics and Astronomy; Lawrence Berkeley National Laboratory, Materials Sciences Division Qian, Kun; Shanghai Jiao Tong University Zhang, Quanzeng; Shanghai Jiao Tong University, Zhou, Guanqing; Shanghai Jiao Tong University Zhang, Ming; Shanghai Jiao Tong University Zhu, Lei; Shanghai Jiao Tong University Qiu, Chaoqun; Shanghai Jiao Tong University Xu, Jinqiu; Chinese Academy of Sciences Fujian Institute of Research on the Structure of Matter Wang, Jing; Shanghai Jiao Tong University Haider, Rizwan; Shanghai Jiao Tong University Feng, Wei; National Key Laboratory of Fluorinated Materials Hu, Hailin; Instituto de Energías Renovables Zhu, Haiming; Department of Chemistry, Zhejiang University Zhang, Yongming; Shanghai Jiao Tong University, Liu, Feng; Shanghai Jiao Tong University,

Control of aggregation and dissolution of small molecules hole transport layer through a doping strategy of highly efficient perovskite solar cell

Jazib Ali[1], Jingnan Song[1], Yu Li[1,*], Kun Qian[1], Quanzeng Zhang[1], Guanqing Zhou[1], Ming Zhang[1], Lei Zhu[2], Chaoqun Qiu[1], Jinqiu Xu[1],Jing Wang[1,*], Rizwan Haider[2], Wei Feng[5], Hailin Hu[6], Haiming Zhu[4],Yongming Zhang[2], Feng Liu[1,2,3,*]

[1]School of Physics and Astronomy, and Collaborative Innovation Center of IFSA (CICIFSA), Shanghai Jiao Tong University, 200240, Shanghai, China.

[2]Department of Polymer Science and Engineering, School of Chemistry and Chemical Engineering, Shanghai Jiao Tong University, Shanghai 200240, P. R. China.

[3]Center for Advanced Electronic Materials and Devices, Shanghai Jiao Tong University, 200240, Shanghai, China.

[4]Department of Chemistry, Zhejiang University, Hangzhou 310027, P.R. China

[5]State Key Laboratory of Fluorinated Materials, Zibo City, Shandong Province 256401, China.

[6]Instituto de Energías Renovables, UNAM, Priv. Xochicalco S/N, Temixco, Morelos, 62580, México.

*Address correspondence to: yu.li@sjtu.edu.cn, wangj1118@sjtu.edu.cn, fengliu82@sjtu.edu.cn

Abstract

Recently, small molecule hole transporting materials (HTLs) have attracted growing interest in perovskite solar cells due to their low-cost, excellent stability and better energy level alignment with perovskite. Nonetheless, an amorphous and coarse surface film is one of the main obstructions to the performance of these small molecule HTLs. Herein, *N,N′*-Di(1-naphthyl)-*N,N′*-diphenyl-(1,1′-biphenyl)-4,4′-diamine (NPB) small molecule was doped with a polymer to overcome the formation of molecular aggregation in HTL. This polymer doping strategy resulted into a very smooth surface, which improved photo-physical and electrochemical properties at HTL/perovskite interface. Consequently, a maximum power conversion efficiency (PCE) of 17.80%, 32% higher than the control, i.e. NPB-based device (13.57%), has been achieved. This work reveals critical behaviour of molecular aggregations on the performance of perovskite solar cells, which impairs the development of an efficient device based on small molecule HTLs.

Key words: NPB, small molecule, PTAA, polymer doping, aggregation, dissolution

Introduction

During last decade, metal halide based perovskite solar cells (PSCs) have been in spotlight due to their promising photovoltaic properties in the variety of device structures[1-3]. As yet, the best reported performance of mesoporous PSCs has reached a certified power conversion efficiency (PCE) of 23.32%[4]. Nevertheless, fabrication of mesoporous PSCs needs high annealing temperature (≥500℃), retarding the development of this emerging flexible module and PSC based monolithic tandem devices[5]. To conquer this issue, researchers developed a planar PSCs structure with a p-i-n and n-i-p (SnO_2-based ETL) structure requiring low-temperature (typically ⩽150℃) solution-processed charge-selective layers[6-8]. Nonetheless, the performance of these planar-structured devices is usually less than that of mesoporous devices[9, 10]. In this regard, numerous striking investigations have already been reported, including various manufacturing techniques[11-13] and interface engineering[7, 10, 14-16], for achieving better performance of planar structured devices.

Large grain size, crystal orientation and morphological defects of perovskite layer, which are critically dependent on the under layer (HTL), are some of the key factors affecting PSC performance[17, 18]. It clinches that the selection of HTLs (e.g. polymer and small molecule) in PSCs is an essential part towards high performance devices. For example, Zheng and co-worker achieved 21% PCE by using a polymer HTL poly[bis(4-phenyl)(2,4,6-trimethylphenyl)amine] (PTAA) along with interfacial modification in the p-i-n PSC[7]. However, small molecule-based HTLs, rather than organic polymers, have well define molecular weight and also versatile with respect to property tuning (hydrophobicity, film morphology, etc.) and demonstrate high batch-to-batch consistency in not only synthesis and purification but also device fabrication[19, 20]. Recently, phenylamine groups containing small molecules have attracted much attraction, because of their high hole mobilities and easily dissolution in common organic solvents. For example, wang *et al*. used 4,4′-cyclohexylidenebis[*N*,*N*-bis(4-methylphenyl) benzenamine] (TAPC) as HTL in the p-i-n PSCs with a highest PCE of 18.8% exemplifying the eminent capacity of small molecule HTLs in PSCs[21]. In addition, another phenylamine group containing organic small molecule NPB[22] has been widely used as HTL in organic light emitting diode (OLED) having good hole mobility around 1×10^3 cm^2/Vs. Therefore, Kim *et al*. first time used this small molecule HTL in PSCs thorough thermal evaporation technique that greatly improved the device V_{oc}, which led to a highest and average PCE of 13.7% and 11.1%, respectively[23]. This NPB HTL film can also be fabricated by spin coating[24, 25], but a highly

rough and non-uniform surface formed after thermal annealing,[26, 27] that was a big hurdle in the way of better performance of NPB based PSCs devices. Despite having all the above properties, PSCs based on small molecule HTLs still display lower performance in comparison with those based on polymer HTLs. A mostly common reason for lower performance of organic small molecules HTLs, have their amorphous film formation ability compared to polymer based HTLs [19, 28-30].

We successfully resolved this issue by using a polymeric doping strategy for small molecule based HTL, leading to improved overall PSC performance. This doping strategy first used in organic thin-film transistors to improve the electronics properties and enhance the nanomorphology of the blend film[8, 31]. Recently, this doping strategy applied on TPAC small molecule HTL in PSCs, which improve the performance of the device to 21%[32] . In this study, NPB was used as HTL. This small molecule was doped with a polymer (PTAA), which efficiently overcame the molecular aggregations in the NPB HTL, leading to a very smooth surface and better energy level alignment with $CH_3NH_3PbI_3$ perovskite by solution processing technique. As a result, the interfacial charge transferability at NPB/$CH_3NH_3PbI_3$ interface were greatly enhanced, contributing to an increase in PSC performance from 13.57% to 17.80%. This work opens up an effective way for producing solution-processed small molecule HTLs with desirable surface morphology in PSCs as well as in OLEDs

2. Results and Discussion

2.1 Working mechanism

Polymers are well known to form films of good quality using solution processing owing to their extended chain formation abilities in dilute solution. These extended chains entangle with each other as the solvent dries out during the spin coating process. Unlike polymers, small molecules show no entanglement because of the lack of extended chain formation ability in the solution and only the packing density can be changed. Therefore, small molecules form very coarse surface after evaporation of solvent. **Figure 1** shows the structural and graphical schematics of the NPB film formation processes with and without PTAA dopant. Specifically, the dissolution of small molecule was supported by the presence of phenyl and methyl groups in the polymer chainwhich contribute to two types of molecular interactions[30]. First is the π-π stacking interaction occurring between the phenyl/phenyl rings in NPB and PTAA respectively, which helps to generate an extended chain length PTAA doped NPB HTL. The second molecular interaction is C–H… π existing between methyl groups[33] of PTAA and the

phenyl rings of the neighbouring NPB. This C–H…p interaction thus interlaces with p–p stacking chains, resulting in a packing motif quite similar to the conformation of polymer chains, thus suppressing intermolecular aggregation and enhance the carrier transport.[30]

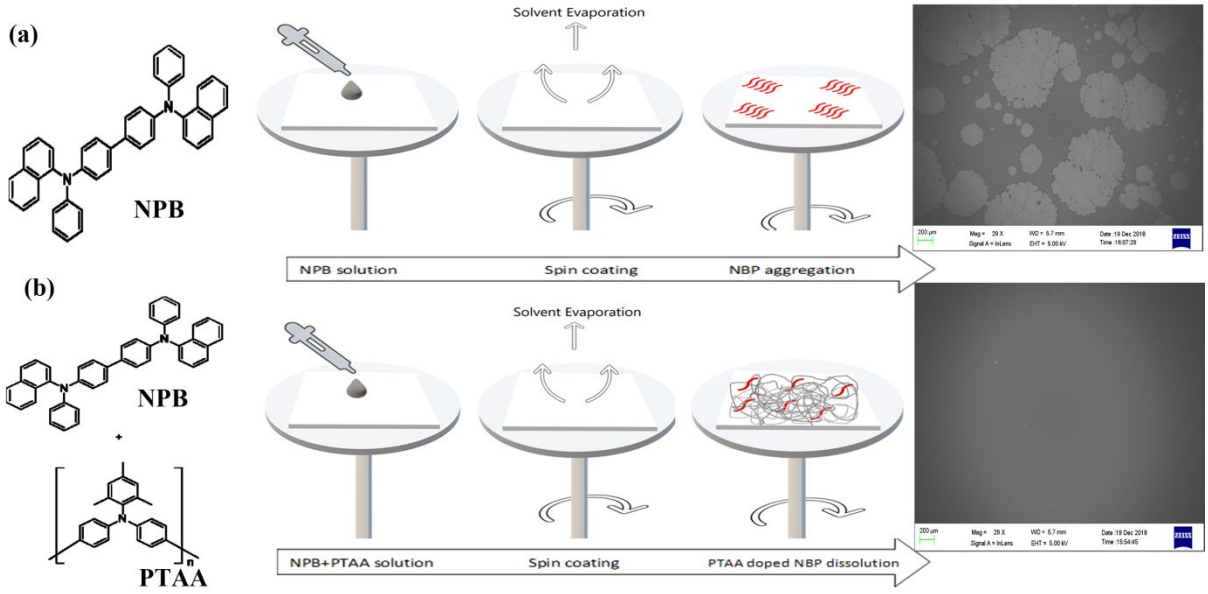

Figure 1. Schematic illustrations of NPB HTL film formation **(a)** without **(b)** with PTAA doping in addition to their related photographs and SEM images.

2.2 Device optimization

Figure 2a,b represents the device configuration of inverted planar heterojunction PSC used in this study. A 10 nm thin PTAA-doped NPB HTL was spin coated on top of an ITO glass followed by a 360 nm thick $CH_3NH_3PbI_3$layer, prepared by a simple 'one step' deposition process. [6,6]-phenyl-C61-butyric acid methyl ester ($PC_{61}BM$, 40 nm) was used as the electron extraction layer atop the perovskite. Finally, a 100 nm thick aluminium (Al) back electrode was deposited by thermal evaporation. Detailed device fabrication is included in the experimental section.

To optimise the amount of PTAA doping, devices were fabricated using different PTAA doping content into the NPB HTL solution. Characteristic current-voltage (*J-V*) curves for full PSCs are displayed in **Figure 2c**, and their PV performance measured under AM 1.5G condition are summarized in **Table 1**. The control device without PTAA doping showed a PCE of 13.58% with an open-circuit voltage (Voc) of 1.03 V, short-circuit current density (*J*sc) of 18.62 mA·cm^{-2} and fill factor (FF) of 70.31 %. Device performance was steadily improved

with the increasing content of PTAA from 0 to 9%, while any further addition of PTAA showed no performance boost. **Figure 2d** shows the *J-V* curve of a champion device with 9% PTAA doping, with V_{OC} of 1.06 V, Jsc of 20.83 mA·cm^{-2}, FF of 80.72% and an overall PCE of 17.80% measured in the reverse direction. PCE decreased a little to 17.08% in forward direction with Voc, Jsc and FF of 1.06 V, 20.62 mA·cm^{-2} and 78.16%, respectively. The devices based on PTAA HTL were also fabricated for comparison, and the Voc is 1.06 V, Jsc 21.00 mA·cm^{2}, FF 76% and PCE 16.89 %. The lower performance of PTAA based devices is ascribed to its lower FF, which might be due to its higher series resistance[34] and unideal wettability as compared to the doped NPB small molecule HTL.

Table 1. Photovoltaic performance of 20 devices of p-i-n PSCs based on different doping content of PTAA into NPB HTL.

Sample	Jsc(mA cm^{-2})	Voc(V)	FF(%)	PCE(%)	Rs(Ω-cm^2)
NPB	*18.62* (17.99±0.63)	*1.03* (1±0.3)	*70.31* (65±5.5)	*13.57* (10±3.57)	10.6
NPB(3%PTAA)	*18.9* (18.4±0.5)	*1.03* (1.01±.02)	*70.5* (67±3.5)	*13.83* (11±3.83)	8.4
NPB(5%PTAA)	*19.54* (19.05±0.49)	*1.05* (1.03±.02)	*76.46* (73±3.6)	*15.87* (12±3.8)	7.25
NPB(7%PTAA)	*19.90* (19.60±0.3)	*1.06* (1.03±.03)	*78.65* (75.25±3)	*16.89* (14±2.9)	5.75
NPB(9%PTAA)	*20.80* (20.09±0.71)	*1.06* (1.04±.02)	*80.72* (78.2±2.5)	*17.79* (16.6±1.2)	5.45
NPB(11%PTAA)	*18.77* (18.23±0.53)	*1.03* (1.02±.02)	*75.71* (73.2±2.5)	*14.73* (13.9±0.83)	7
PTAA	*20.93* (20.33±0.6)	*1.06* (1.03±.03)	*76* (72±4)	*16.89* (15.9±1)	7

Figure 2e shows external quantum efficiency (EQE) and integrated current densities of PSCs at 0 and 9% PTAA doped NPB HTL. A notable improvement in EQE values was observed throughout the UV-Vis range with the corresponding integrated Jsc of 18.27 and 20.59 mA·cm^{-2} at 0 and 9% doping ratio, respectively, in good agreement with Jsc obtained from J-V curve. **Figure 2f** displays the statistical dependence of PCE of 20 devices of PSCs with NPB (0 and 9% PTAA doped) HTLs, showing unambiguously appreciable improvement with proper PTAA dopant. In order to investigate the effect of PTAA on the mixed HTL, a combination of morphological, structural, optical and electrochemical characterization was conducted, which are discussed in following sections.

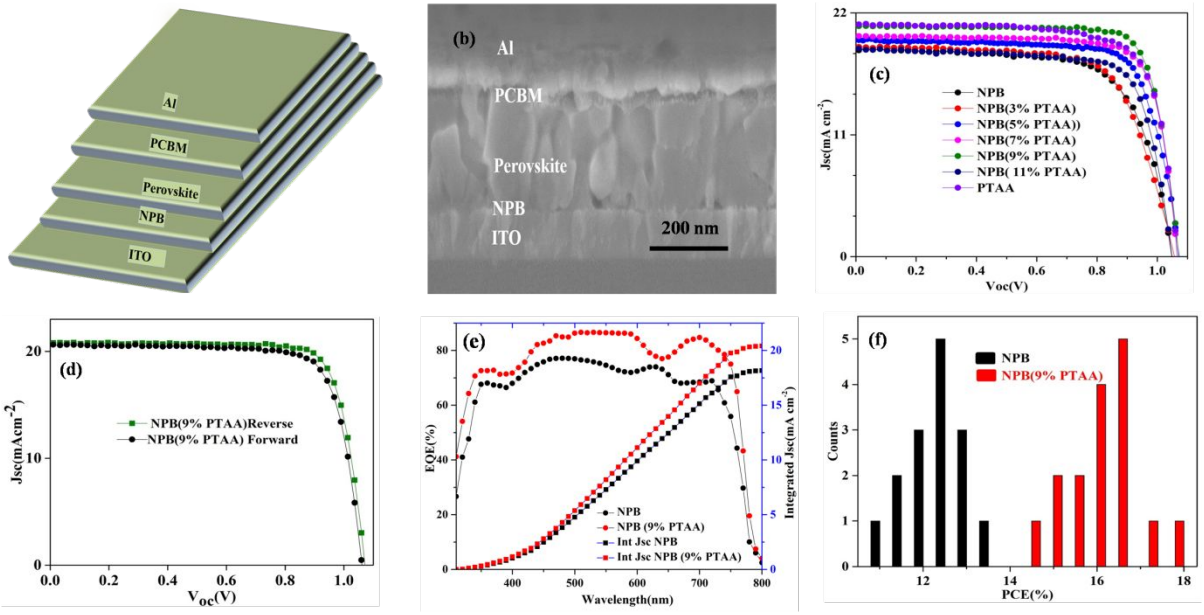

Figure 2. (a) Device configuration of the p-i-n PSCs; (b) SEM cross sectional image of full device; (c) *J–V* curve of perovskite devices fabricated with and without PTAA doped NPB HTLs; (d) *J-V* curve of a champion device measured with forward and reverse scans under simulated AM 1.5G illumination of 100 mW·cm^{-2}; (e) EQE and integrated Jsc of control and NPB (9% PTAA); (f) Statistical performance of 15 perovskite devices on control and NPB (9% PTAA).

2.2 Morphological characterizations

Atomic force microscopy (AFM) was used to investigate the surface morphology of the PTAA doped NPB HTL at an field of view of 5×5 μm^2, shown in **Figure 3**. The root mean-square (RMS) value of pure NPB HTL film was determined to be 12 nm. It decreased to 5, 2.5, 1.4, 0.49 and 0.43 nm after 3%, 5%, 7%, 9% and 11% PTAA doping, respectively. This considerable reduction in RMS value strongly suggests that PTAA molecules were well dispersed within the NPB small molecule matrix due to similar repeating unit structure of both molecules, and molecular aggregation was significantly reduced, which led towards a flat and smooth surface. The smoothness of surface continues improving up to 9%, after which there is no significant change in the RMS value, e.g. the RMS value was 0.49 nm and 0.43 nm for 9% and 11% PTAA doping, respectively, indicating that at 9% PTAA doping the morphology reached almost its optimization value, so that any further increase in doping ratio had no obvious effect on the RMS value. Thus, these AFM results support the fact that doping of PTAA into the NPB small molecule efficiently enhances the film uniformity by overcoming

the molecular aggregation of NPB small molecule which helps to create a better contact between HTL and perovskite by mitigating surface trap states, resulting a better V_{oc} and FF[35, 36].

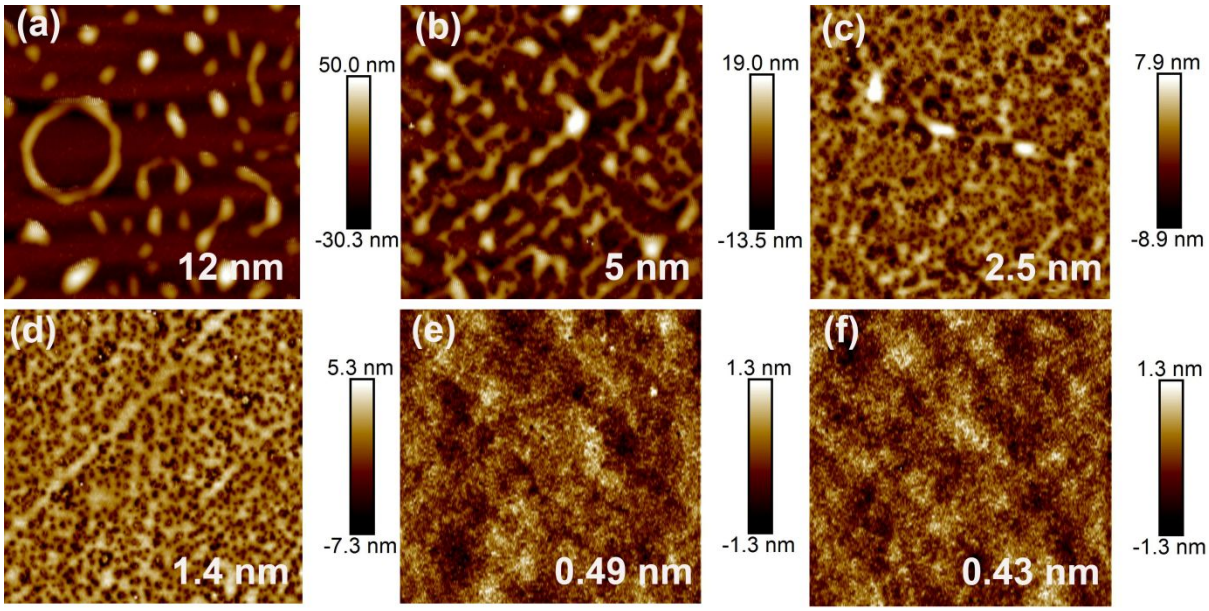

Figure 3. AFM top view image of PTAA-doped NPB film: (a) No doping; (b) 3% PTAA; (c)5% PTAA; (d) 7% PTAA; (e)9% PTAA; (f) 11% PTAA.

To explore the wetting capability of NPB HTLs, we measured water contact angle (insets in **Figure 4).** The water contact angle of pure NPB HTL was 69°, but it increased with increasing the PTAA doping content, e.g. 81° for 9 or 11% doping. The increment in water contact angle after PTAA doping is possibly due to increasing in the length of hydrophobic alkyl chain of NPB small molecules, resulting into surface being more hydrophobic[37]. Thus, the higher water contact angles induced by PTAA doping proposed a reduction in nucleation sites, which ultimately resulted into larger grain size and improved perovskite layer quality[38, 39].

Figure 4 represents the top view SEM images of the perovskite films on NPB HTLs. It is clear that perovskite films on the doped HTLs show larger grain size than that of the control film. The average grain size of perovskite on pure NPB HTL was 380 nm, and it increased to 430, 442, 445, 467 and 466 nm after 3, 5, 7, 9, 11% PTAA doping, respectively. The largest grain size on 9% PTAA doped NPB completely correlate with the best performance of our device of 17.80%. This entails that the carriers can effectively transport across the perovskite films and reach the corresponding electrode interfaces before recombination occurs [40]. The foregoing surface morphologies indicate that the PTAA doping into NPB small molecule can improve

HTL film smoothness and enhance perovskite grain size as well, the two important requirements for high performance in PSCs.

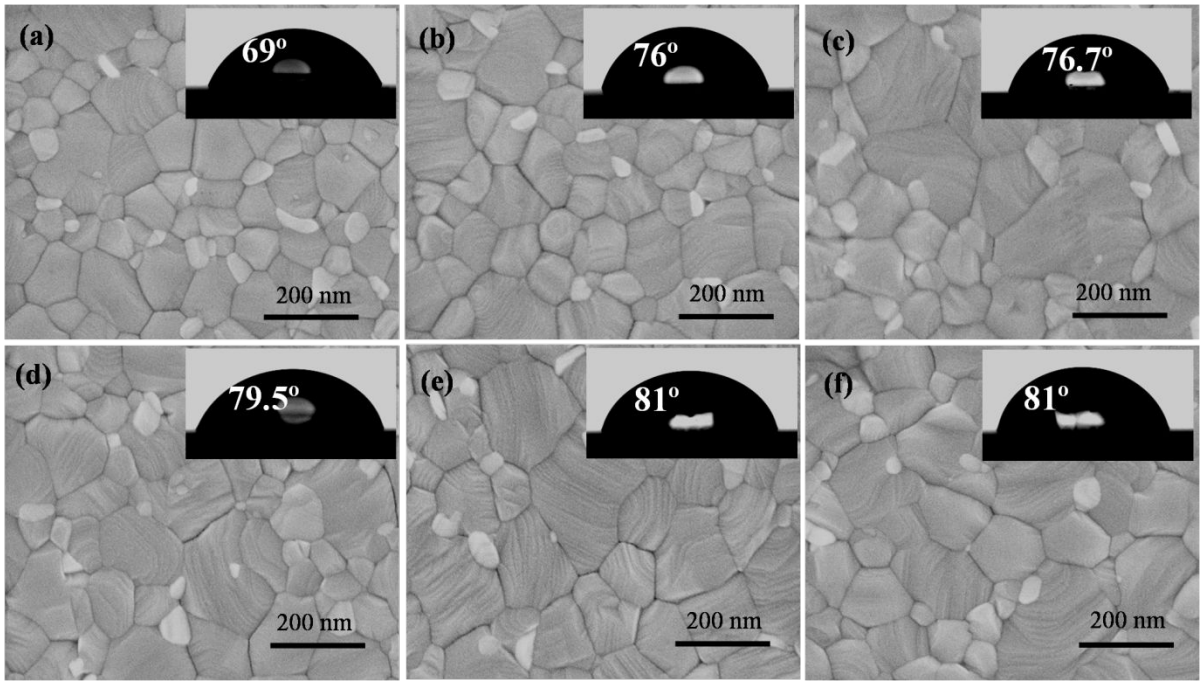

Figure 4. SEM top view image of $CH_3NH_3PbI_3$ layer on NPB with (a) no doping, (b) 3% PTAA, (c) 5% PTAA, (d) 7% PTAA, (e) 9% PTAA, and (f) 11% PTAA, respectively.

2.3 Structural and spectroscopic characterizations

To explore the influence of PTAA doped small molecule HTL on perovskite crystallization, grazing incidence wide angle X-ray diffraction (GIWAXS) technique was applied. The scattering patterns of films were collected by a 2D detector, in which perovskite crystallite orientation are well characterized. **Figure S1** illustrates the GIWAX profiles of perovskite films including in-plane Q_{xy} and out-of-plane Q_z, where $Q = 4\pi\sin\theta/\lambda$, where θ is half of the scattering angle and X-ray wavelength λ=0.124 nm. These strongly scattered pattern rings exhibits that the crystal domains are predominately polycrystalline as reported in literatures[41, 42], and such crystallographic orientations of perovskite film remain intact during film fabrication on the control or doped NPB HTL. **Figure 5a** shows the scattering intensities integrated over the scattering vector q, which gives 1D GIWAX patterns of perovskite films. The position of the peaks at 1.0, 2.0 and 2.3 $Å^{-1}$ can be attributed to the (110), (220), and (310) lattice planes respectively and are in same positions for all the $CH_3NH_3PbI_3$ thin films, which stipulate that all of the perovskite peaks have tetragonal crystal structures[43]. However, the perovskite film coated on doped HTLs exhibits sharper and stronger peaks as compared to pure

NPB HTL, indicating better crystallinity and highly ordered perovskite crystals with lower defects in NPB doped perovskite films. Moreover, it was found that the perovskite thin films based on the doped NPB HTL show larger crystal size as compared to pure NPB film as shown in **Figure 5b**. Notably, the 9% doping of PTAA shows comparatively stronger intensity around (110) plane, indicating that the perovskite crystals formation on that surface have higher orientation compared to the control and other PTAA doped NPB HTL.

To investigate the effect of PTAA doping onto the energy level of NPB small molecule, ultraviolet photoelectron spectroscopy (UPS) was performed. **Figure 5c and S2** show highest occupied molecular orbital (HOMO) of the mixed HTLs, which reveals that the energy levels of the NPB HTL after 0 to11% PTAA doping change the HOMO of NPB from 5.39, 5.40, 5.41, 5.44, 5.46, to 5.38 eV, respectively. The highest energy level offset obtained at 11% PTAA doping between valence band of perovskite and HOMO level of mixed HTL, is the main cause of performance decreasing beyond 9% PTAA doping. This variation in HOMO levels of mixed HTL suggests an orientation change of NPB, as it has already been proved that the energy level of organic thin film is largely influenced by the change in molecular orientation[32, 44]. So, the 9% PTAA doped NPB energetically agrees well with the $CH_3NH_3PbI_3$ film, demonstrating efficient charge transfer between the perovskite and the mixed NPB HTL. The similarity in HOMO energy levels also helps to reduce energy losses at the interface contact which leads to a higher V_{oc}[45,46]. Moreover, these UPS results completely support the dependence of V_{oc} on the energy band alignment after PTAA doping into the NPB HTL.

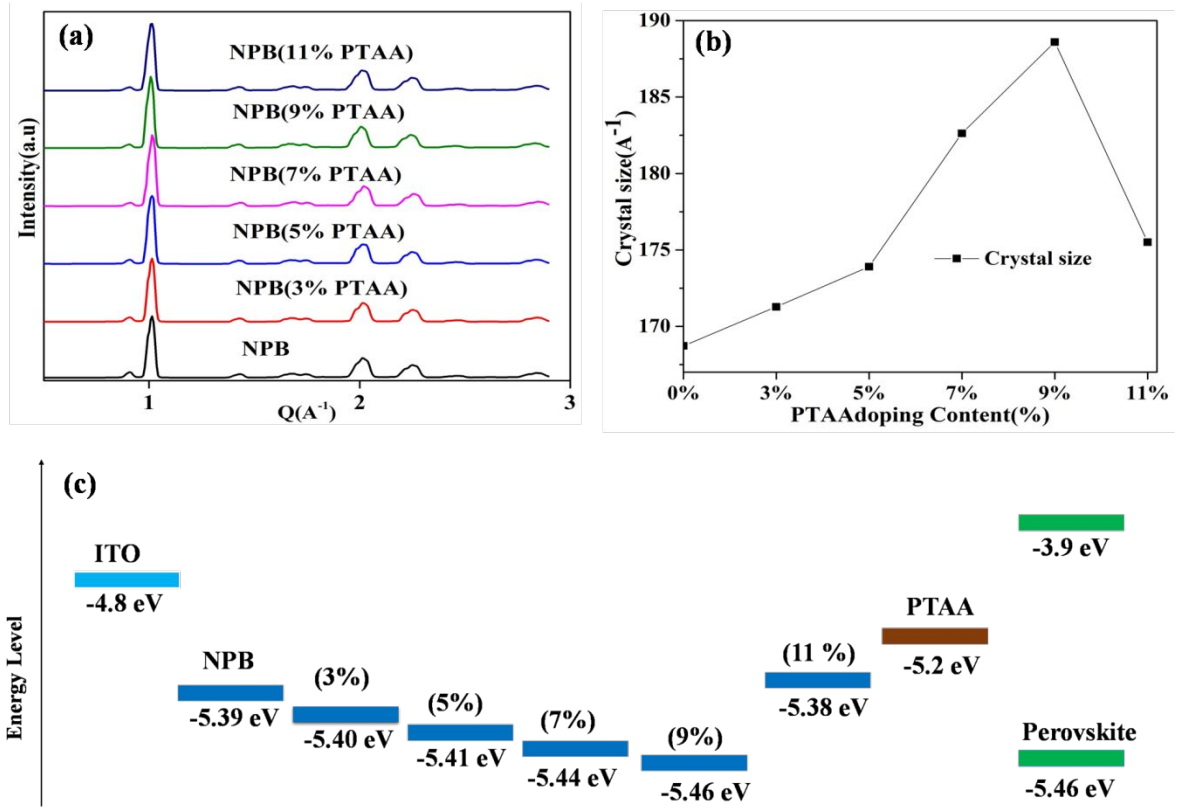

Figure 5. (a) GIWAX scattering profile of $CH_3NH_3PbI_3$ film on control and doped NPB HTL; (b) Crystal size of perovskite film at diffrent doping content of PTAA in NPB HTL; (c) Energy levels of perovskite and NPB with different doping content of PTAA.

In PSCs, fully absorbing the solar irradiance is critical for high device performance. Here, it was observed that perovskite film morphological improvements induced appreciable enhancement in its UV-visible absorption spectrum. **Figure S3** shows the UV-visible absorbance spectra of $CH_3NH_3PbI_3$ on the control and doped NPB films. All PTAA doped NPB films exhibited better light absorption in the range of 400 to 800 nm as compared to the control NPB film.

The effect of PTAA doping on the hole mobility of NPB small molecule was investigated by space charge limiting current (SCLC) technique. **Figure S4** shows the device structure and the *J-V* curves for SCLC. Here, this linear part at high bias voltage of the curve represents the SCLC region. According to the Mott-Gurney law[9] $J \propto V_a^2$, a larger slope means a higher mobility. We can see that the mobility of the control and 9% PTAA doped NPB samples are

1.56×10^{-3} and 3.62×10^{-3} cm^2/S respectively, suggesting that PTAA doping in NPB had minor effect on the hole mobility.

Furthermore, the efficient charge carrier extraction ability was explore by the steady-state photoluminescence (PL) and time-resolved PL (TRPL) spectroscopy[10]. Here, an ITO/HTL/perovskite structure was used to perform these characterizations. **Figure 6a** displays PL spectra of perovskite films on pure and PTAA doped NPB HTLs where a characteristic emission peak at 770 nm can be seen. Moreover, in each case the PL emission is considerably weaker as compared to that from the pure NPB sample, indicating superior interfacial charge transfer. It is exciting that the PL quenching capability largely depends on the doping ratio, e.g. the major PL quenching experienced was at 9% PTAA doping. Any further increase in doping ratio beyond 9% will rise up the intensity of PL curve which can be due to mismatch of energy level alignment[47]. This obvious quenching exhibits a reduction in charge recombination, resulting an improved hole collection ability in the mixed HTLs. Next, TRPL measurements were performed to further elaborate the lifetime of charge carrier in pure and doped NPB HTL. The observed TRPL decays were fitted with a bi-exponential decay function

$$f(t)=A_1\exp(-t/\tau_1) + A_2\exp(-t/\tau_2)$$

where τ_1 and τ_2 is the fast and slow decay time, while A_1 and A_2 represents decay amplitude of fast and slow recombination, respectively[48]. The fast decay curve component is a result of charge carriers quenched by charge extraction layer and slow decay curve component originates from radiative bimolecular recombination[49]. **Figure 6b** displays that the lifetime of fast decay component decreases from 8 ± 0.058 ns to 5.5 ± 0.091, 5.10 ± 0.061, 4.75 ± 0.089, 4.30 ± 0.06 and 5.18 ± 0.108 ns after 3, 5, 7, 9 and 11% PTAA doping, respectively. The above results advocate fast and efficient hole extraction at the HTL/perovskite interface after PTAA doping[50], which is mainly attributed to the better energy level alignment and also to the better mobility that has been achieved after better crystallizations of doped NPB HTL[51]. The results obtained from optical measurements are clearly dependent on the PTAA-doping ratio. The largest PL quenching as well as fast decay lifetime observed at 9% doping ratio of PTAA supports the highest holes extraction efficiency. Moreover, the high FF and Jsc further proves the efficient charge transfer and extraction of such a planar p-i-n heterojunction PSCs.

For detailed understanding of photo excited charge carrier dynamics in the HTL/Perovskite bilayers, transient absorption spectroscopy (TAS) studies were performed. **Figure 6c** exhibits

the pseudo-color TA plot of the differential transmission (ΔT/T) as a function of wavelength and time for perovskite film. The main ΔT/T peak at ~750 nm is recognized to the transient photo induced bleaching[52-54] and similar peaks are observed in **Figure 6d,** when perovskite film is excited at time delays from 0.1 ps to 10000 ps. Moreover, the kinetic decay traces of photo bleaching features are presented in **Figure 6e**, in which the slow rising phase in TA signal could be the cooling process of hot excitons, due to the vibrational relaxation[55]. The single fitted exponential function represents the comparison of perovskite spectra on pure and doped NPB HTL, which gives valuable information about the charge extraction from perovskite to HTLs. The fitted results of pure NPB based perovskite film show the decay time constant τ 196.35 ± 1.98 ps, but after 3, 5, 7, 9 and 11% PTAA doping it is efficiently reduced to 193.16 ± 1.62, 177.27 ± 1.01, 167.61 ± 1.12, 164.04 ± 1.26 and 182.08 ± 0.75 ps, respectively. The lowest decay time achieved after 9% PTAA doping suggests strongest electronic coupling between perovskite and NPB after 9% PTAA doping, which leads to fastest charge transfer between perovskite and doped NPB HTL.

To further explore the charge carrier dynamics on the whole perovskite device, electrochemical impedance spectroscopic (EIS) measurements were performed. This powerful technique is very helpful for the investigation of charge transportation properties within the materials and at PSC interfaces[56-61]. The impedance associated with the interfaces can be determined using EIS with a small AC voltage perturbation in the working device and a gradual frequency change from high to low. **Figure 6f** shows the Nyquist plot of IS with an equivalent circuit model representing the inner series resistances of the device. R_{sheet}, $R_{tranport}$ representing the sheet resistance of the cell and charge carrier transport resistance at the interfaces, respectively. The fitted values of R_{sheet} are evidently suppressed upon PTAA doping from 3.9 (control) to 2.5K·Ohm·cm^2 with 9% PTAA doping that PTAA doping effectively improved the conductivity of the of NPB small molecule[62]. However, the reduction of $R_{transport}$ from 2029 (control) to 129 K·Ohm·cm^2 at 9% doping indicates that the PTAA doping strategy accelerates the charge carrier transport and is also helpful in minimization of energy loss during the charge collection process[63, 64].The lowest values of both R_{sheet} and $R_{tranport}$ are achieved at 9% doping ratio and any further increase in doping ratio increases both resistances, which is highly

consistent with other results.

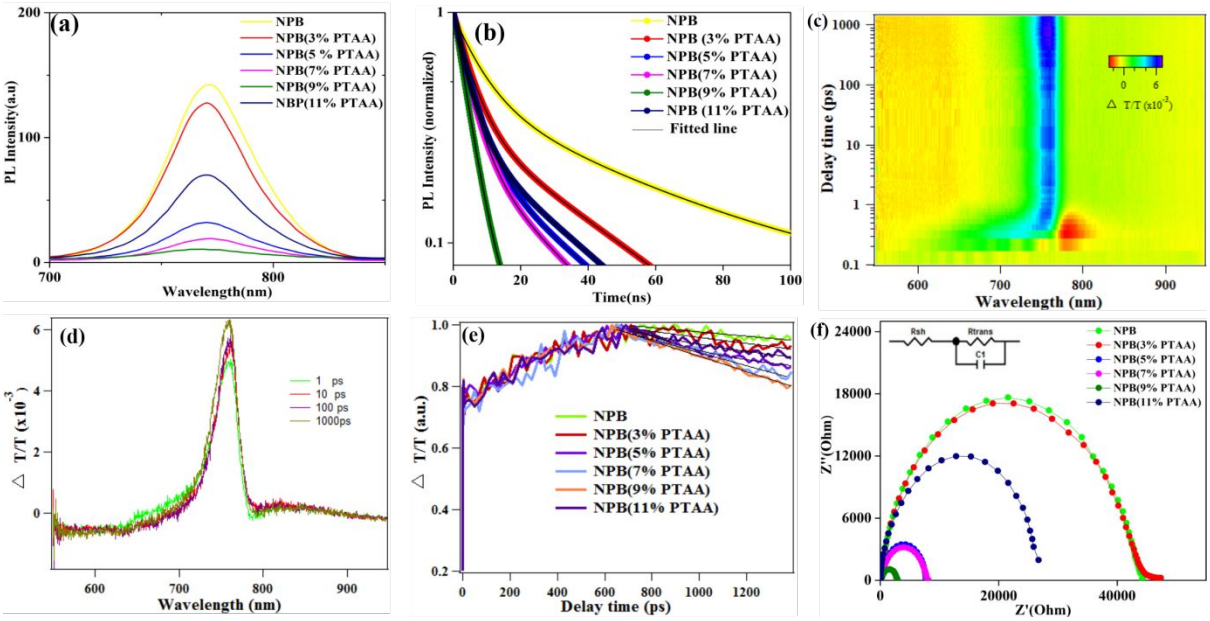

Figure 6. (a) Steady-state PL spectra of perovskite on NPB (with and without doping) HTLs; (b) TRPL spectra of perovskite film on NPB (with and without doping) HTLs; (c) 2D psuedo color image of the TA spectrum for a $CH_3NH_3PbI_3$ film; (d) fs-TA spectra of perovskite at time delays from 0.1 ps to 10000 ps; (e)Normalized bleaching kinetics of perovskite film on NPB (with and without doping) HTL at 770 nm; (f) Nyquist plot of PSCs on NPB (with and without doping) HTL.

2.4 Stability

Lower stability is one of the biggest hurdles for PSCs commercialisation. It was noticed that perovskite device stability on PTAA doped NPB small molecule was better than the pure NPB devices. Stability of Perovskite devices based on the control and doped NPB HTLs was tested under the relative humidity of 60% at room temperature for 150 h. The doped NPB HTL based PSCs maintained the initial performance over 90%, whereas the PCSs using the pure NPB showed a decrease to less than 70%. The assessment of normalized Voc, Jsc, FF and PCE of doped and undoped NPB based PSCs were presented in **Figure 7a-d**, which shows that the doping of PTAA into NPB significantly improved the perovskite device stability. Compared with the control devices, the doped NPB perovskite solar cells presented better stability against degradation in ambient air after 20 days without encapsulations as shown in **Figure S5**, which demonstrates the adaptability of our approach for PSCs. One of the possible reasons for such outstanding ambient air stability could be ascribed to hydrophobic nature of doped NPB layer.[65] The larger water contact angle suggesting the better moisture resistivity of doped NPB

compared to the control NPB. The hydrophobic characteristic of doped NPB can prevent moisture penetrating the perovskite film, which led to improved ambient stability.

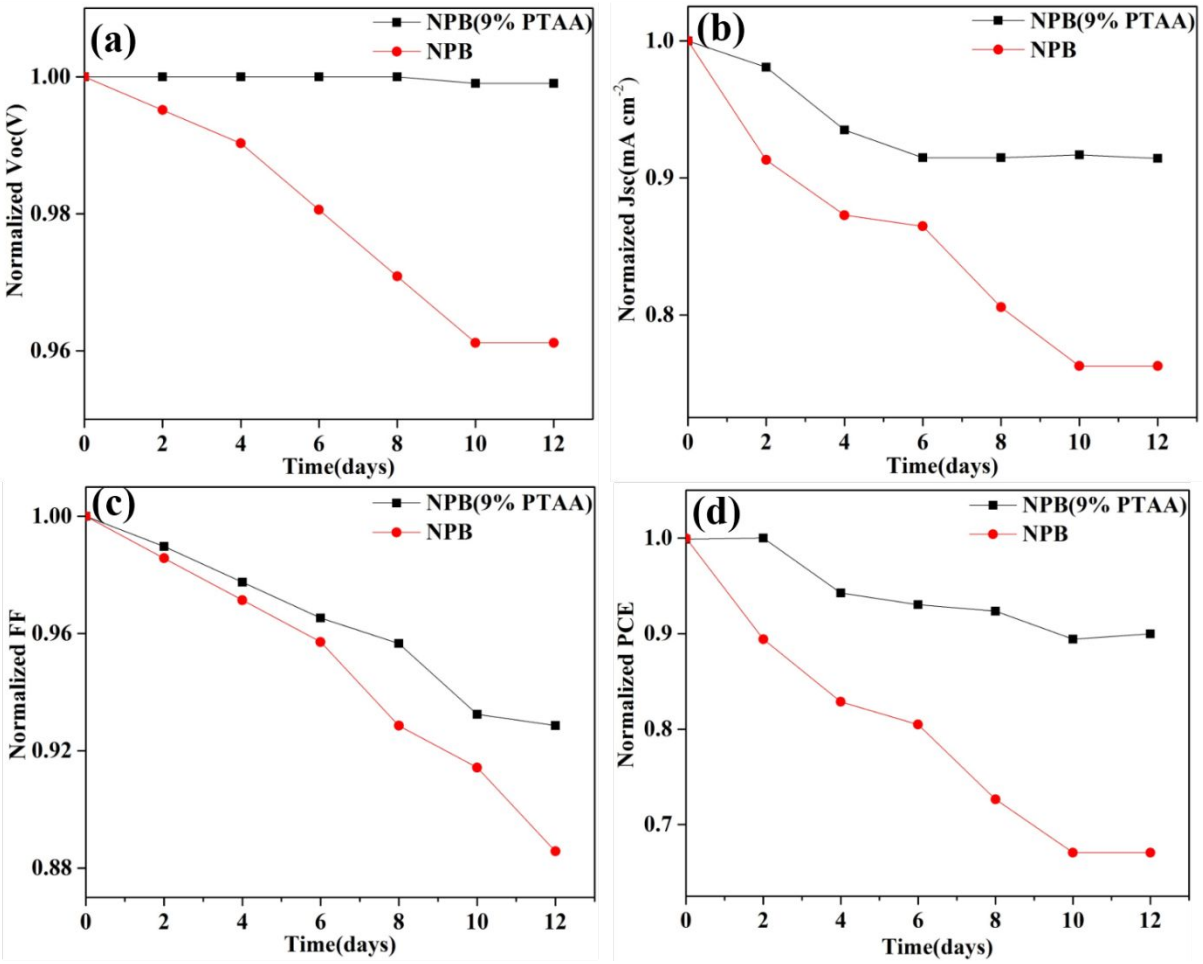

Figure 7. Storage stability tests of perovskite devices based on NPB(control and 9% doping)HTL: Normalized (a)Voc; (b) JSC; (c) FF; (d) PCE.

3.Conclusion

In conclusion, we have successfully developed a polymer-small molecule doping strategy to improve the dissolution of small molecules, leading to defeat the molecular aggregation in its structure, which resulted into a formation of uniform and smooth HTL with better crystallinity. This polymer doping strategy improves the energy level alignment between small molecule HTL and valence band of perovskite. Therefore, a superior charge transfer occurs at HTL/perovskite interface with reduced charge transport resistance. As a result, a valuable up gradation was achieved for device Jsc and FF. With increasing the PTAA doping content, the device performance increased up to 9% and any further increase in doping content declined the device performance. This drop down of performance was mainly due to the energy level offset

between HTL and perovskite after 9% PTAA doping. This strategy enables us to get the highest performance reaches to 17.80%. This study provides a simple and efficacious protocol to improve the performance of PSCs based on the PTAA doped small molecule HTLs.

Conflicts of Interest

There are no conflicts of interest to declare.

Acknowledgements

This work was financially supported by the Young 1000 Talent Program of China, the National Natural Science Foundation of China (NSFC) (Nos. 21734009, 51473009, 21225209, 91427303, and BC0720230), PAPIIT-UNAM (IN102619) (Mexico) and CONACyT-Fronteras de la Ciencia 2016-2024 (Mexico). Portions of this research were carried out at beam line 7.3.3 at the Advanced Light Source, Molecular Foundry, Lawrence Berkeley National Laboratory, which was supported by the DOE, Office of Science, and Office of Basic Energy Sciences.

Experimental detail avalible in suplimentry section

Reference

1. Kojima, A.; Teshima, K.; Shirai, Y.; Miyasaka, T., Organometal halide perovskites as visible-light sensitizers for photovoltaic cells. *Journal of the American Chemical Society* **2009,** *131* (17), 6050-6051.
2. Liu, M.; Johnston, M. B.; Snaith, H. J., Efficient planar heterojunction perovskite solar cells by vapour deposition. *Nature* **2013,** *501* (7467), 395.
3. Qiu, J.; Qiu, Y.; Yan, K.; Zhong, M.; Mu, C.; Yan, H.; Yang, S., All-solid-state hybrid solar cells based on a new organometal halide perovskite sensitizer and one-dimensional TiO 2 nanowire arrays. *Nanoscale* **2013,** *5* (8), 3245-3248.
4. Jiang, Q.; Zhao, Y.; Zhang, X.; Yang, X.; Chen, Y.; Chu, Z.; Ye, Q.; Li, X.; Yin, Z.; You, J., Surface passivation of perovskite film for efficient solar cells. *Nature Photonics* **2019**.
5. Bi, C.; Chen, B.; Wei, H.; DeLuca, S.; Huang, J., Efficient Flexible Solar Cell based on Composition-Tailored Hybrid Perovskite. *Advanced Materials* **2017,** *29* (30), 1605900.
6. Jeng, J. Y.; Chiang, Y. F.; Lee, M. H.; Peng, S. R.; Guo, T. F.; Chen, P.; Wen, T. C., CH3NH3PbI3 perovskite/fullerene planar-heterojunction hybrid solar cells. *Advanced Materials* **2013,** *25* (27), 3727-3732.
7. Zheng, X.; Chen, B.; Dai, J.; Fang, Y.; Bai, Y.; Lin, Y.; Wei, H.; Zeng, X. C.; Huang, J., Defect passivation in hybrid perovskite solar cells using quaternary ammonium halide anions and cations. *Nature Energy* **2017,** *2* (7), 17102.
8. Jiang, Q.; Zhang, L.; Wang, H.; Yang, X.; Meng, J.; Liu, H.; Yin, Z.; Wu, J.; Zhang, X.; You, J., Enhanced electron extraction using SnO2 for high-efficiency planar-structure HC(NH2)2PbI3-based perovskite solar cells. *Nature Energy* **2016,** *2*, 16177.

9. Huang, Z.; Hu, X.; Liu, C.; Tan, L.; Chen, Y., Nucleation and crystallization control via polyurethane to enhance the bendability of perovskite solar cells with excellent device performance. *Advanced Functional Materials* **2017,** *27* (41), 1703061.
10. Zhou, Z.; Li, X.; Cai, M.; Xie, F.; Wu, Y.; Lan, Z.; Yang, X.; Qiang, Y.; Islam, A.; Han, L., Stable Inverted Planar Perovskite Solar Cells with Low-Temperature-Processed Hole-Transport Bilayer. *Advanced Energy Materials* **2017,** *7* (22), 1700763.
11. Liao, H. C.; Guo, P.; Hsu, C. P.; Lin, M.; Wang, B.; Zeng, L.; Huang, W.; Soe, C. M. M.; Su, W. F.; Bedzyk, M. J., Enhanced Efficiency of Hot-Cast Large-Area Planar Perovskite Solar Cells/Modules Having Controlled Chloride Incorporation. *Advanced Energy Materials* **2017,** *7* (8), 1601660.
12. Chiang, C.-H.; Nazeeruddin, M. K.; Grätzel, M.; Wu, C.-G., The synergistic effect of H 2 O and DMF towards stable and 20% efficiency inverted perovskite solar cells. *Energy & Environmental Science* **2017,** *10* (3), 808-817.
13. Luo, D.; Zhao, L.; Wu, J.; Hu, Q.; Zhang, Y.; Xu, Z.; Liu, Y.; Liu, T.; Chen, K.; Yang, W., Dual-Source Precursor Approach for Highly Efficient Inverted Planar Heterojunction Perovskite Solar Cells. *Advanced Materials* **2017,** *29* (19), 1604758.
14. Wang, Q.; Dong, Q.; Li, T.; Gruverman, A.; Huang, J., Thin Insulating Tunneling Contacts for Efficient and Water-Resistant Perovskite Solar Cells. *Advanced Materials* **2016,** *28* (31), 6734-6739.
15. Yang, L.; Cai, F.; Yan, Y.; Li, J.; Liu, D.; Pearson, A. J.; Wang, T., Conjugated Small Molecule for Efficient Hole Transport in High-Performance p-i-n Type Perovskite Solar Cells. *Advanced Functional Materials* **2017,** *27* (31), 1702613.
16. Bao, X.; Wang, J.; Li, Y.; Zhu, D.; Wu, Y.; Guo, P.; Wang, X.; Zhang, Y.; Wang, J.; Yip, H. L., Interface Engineering of a Compatible PEDOT Derivative Bilayer for High-Performance Inverted Perovskite Solar Cells. *Advanced Materials Interfaces* **2017,** *4* (6), 1600948.
17. Chen, J.; Shi, T.; Li, X.; Zhou, B.; Cao, H.; Wang, Y., Origin of the high performance of perovskite solar cells with large grains. *Applied Physics Letters* **2016,** *108* (5), 053302.
18. Wang, Z.-K.; Gong, X.; Li, M.; Hu, Y.; Wang, J.-M.; Ma, H.; Liao, L.-S., Induced crystallization of perovskites by a perylene underlayer for high-performance solar cells. *ACS nano* **2016,** *10* (5), 5479-5489.
19. Schloemer, T. H.; Christians, J. A.; Luther, J. M.; Sellinger, A., Doping strategies for small molecule organic hole-transport materials: impacts on perovskite solar cell performance and stability. *Chemical Science* **2019,** *10* (7), 1904-1935.
20. Shang, R.; Zhou, Z.; Nishioka, H.; Halim, H.; Furukawa, S.; Takei, I.; Ninomiya, N.; Nakamura, E., Disodium Benzodipyrrole Sulfonate as Neutral Hole-Transporting Materials for Perovskite Solar Cells. *Journal of the American Chemical Society* **2018,** *140* (15), 5018-5022.
21. Yang, L.; Cai, F.; Yan, Y.; Li, J.; Liu, D.; Pearson, A. J.; Wang, T., Conjugated Small Molecule for Efficient Hole Transport in High-Performance p-i-n Type Perovskite Solar Cells. *Advanced Functional Materials* **2017,** *27* (31), 1702613.
22. Van Slyke, S. A.; Chen, C.; Tang, C. W., Organic electroluminescent devices with improved stability. *Applied physics letters* **1996,** *69* (15), 2160-2162.
23. Kim, B.-S.; Kim, T.-M.; Choi, M.-S.; Shim, H.-S.; Kim, J.-J., Fully vacuum–processed perovskite solar cells with high open circuit voltage using MoO3/NPB as hole extraction layers. *Organic Electronics* **2015,** *17*, 102-106.
24. Kim, K.-H.; Huh, S.-Y.; Seo, S.-m.; Lee, H. H., Solution-based formation of multilayers of small molecules for organic light emitting diodes. *Applied Physics Letters* **2008,** *92* (9), 76.
25. Ishihara, M.; Okumoto, K.; Shirota, Y., Pronounced Effect of the Methods of Preparation of Organic Thin Films on Hole Injection from the Indium-tin-oxide Electrode–Vacuum Deposition vs Spin Coating. *Chemistry letters* **2003,** *32* (2), 162-163.
26. Park, J. J.; Park, T. J.; Jeon, W. S.; Pode, R.; Jang, J.; Kwon, J. H.; Yu, E.-S.; Chae, M.-Y., Small molecule interlayer for solution processed phosphorescent organic light emitting device. *Organic Electronics* **2009,** *10* (1), 189-193.
27. Kim, D.-H.; Choi, D. H.; Park, J. J.; Lee, S. T.; Kwon, J. H., Novel Green Small-molecule Host Materials for Solution-processed Organic Light-emitting Diodes. *Chemistry letters* **2008,** *37* (11), 1150-1151.

28. Smith, J.; Heeney, M.; McCulloch, I.; Malik, J. N.; Stingelin, N.; Bradley, D. D.; Anthopoulos, T. D., Percolation behaviour in high mobility p-channel polymer/small-molecule blend organic field-effect transistors. *Organic Electronics* **2011,** *12* (1), 143-147.
29. Liu, C.; Qiu, Z.; Li, F.; Meng, W.; Yue, W.; Zhang, F.; Qiao, Q.; Wang, M., From binary to multicomponent photoactive layer: A promising complementary strategy to efficient hybrid solar cells. *Nano Energy* **2015,** *12*, 686-697.
30. Duan, L.; Hou, L.; Lee, T.-W.; Qiao, J.; Zhang, D.; Dong, G.; Wang, L.; Qiu, Y., Solution processable small molecules for organic light-emitting diodes. *Journal of Materials Chemistry* **2010,** *20* (31), 6392-6407.
31. Hwang, H.; Park, S.; Heo, J. H.; Kim, W.; Ahn, H.; Kim, T.-S.; Im, S. H.; Son, H. J., Enhancing performance and stability of perovskite solar cells using hole transport layer of small molecule and conjugated polymer blend. *Journal of Power Sources* **2019,** *418*, 167-175.
32. Li, W.; Liu, C.; Li, Y.; Kong, W.; Wang, X.; Chen, H.; Xu, B.; Cheng, C., Polymer Assisted Small Molecule Hole Transport Layers Toward Highly Efficient Inverted Perovskite Solar Cells. *Solar RRL* **2018,** *2* (11), 1800173.
33. Qiao, J.; Wang, L. D.; Xie, J. F.; Lei, G. T.; Wu, G. S.; Qiu, Y., Strongly luminescent binuclear aluminium chelate with polymer-like molecular packing and solution-processibility. *Chemical Communications* **2005,** (36), 4560-4562.
34. Wang, Q.; Bi, C.; Huang, J., Doped hole transport layer for efficiency enhancement in planar heterojunction organolead trihalide perovskite solar cells. *Nano Energy* **2015,** *15*, 275-280.
35. Huang, X.; Wang, K.; Yi, C.; Meng, T.; Gong, X., Efficient perovskite hybrid solar cells by highly electrical conductive PEDOT: PSS hole transport layer. *Advanced Energy Materials* **2016,** *6* (3), 1501773.
36. Liang, Y.; Xu, Z.; Xia, J.; Tsai, S. T.; Wu, Y.; Li, G.; Ray, C.; Yu, L., For the bright future—bulk heterojunction polymer solar cells with power conversion efficiency of 7.4%. *Advanced materials* **2010,** *22* (20), E135-E138.
37. Zhang, J.; Hu, Z.; Huang, L.; Yue, G.; Liu, J.; Lu, X.; Hu, Z.; Shang, M.; Han, L.; Zhu, Y., Bifunctional alkyl chain barriers for efficient perovskite solar cells. *Chemical Communications* **2015,** *51* (32), 7047-7050.
38. Bi, C.; Wang, Q.; Shao, Y.; Yuan, Y.; Xiao, Z.; Huang, J., Non-wetting surface-driven high-aspect-ratio crystalline grain growth for efficient hybrid perovskite solar cells. *Nature communications* **2015,** *6*, 7747.
39. Huang, C.; Fu, W.; Li, C.-Z.; Zhang, Z.; Qiu, W.; Shi, M.; Heremans, P.; Jen, A. K.-Y.; Chen, H., Dopant-Free Hole-Transporting Material with a C 3 h Symmetrical Truxene Core for Highly Efficient Perovskite Solar Cells. *Journal of the American Chemical Society* **2016,** *138* (8), 2528-2531.
40. Deng, Y.; Peng, E.; Shao, Y.; Xiao, Z.; Dong, Q.; Huang, J., Scalable fabrication of efficient organolead trihalide perovskite solar cells with doctor-bladed active layers. *Energy & Environmental Science* **2015,** *8* (5), 1544-1550.
41. Tan, K. W.; Moore, D. T.; Saliba, M.; Sai, H.; Estroff, L. A.; Hanrath, T.; Snaith, H. J.; Wiesner, U., Thermally induced structural evolution and performance of mesoporous block copolymer-directed alumina perovskite solar cells. *ACS nano* **2014,** *8* (5), 4730-4739.
42. Huang, W.; Huang, F.; Gann, E.; Cheng, Y. B.; McNeill, C. R., Probing Molecular and Crystalline Orientation in Solution-Processed Perovskite Solar Cells. *Advanced Functional Materials* **2015,** *25* (34), 5529-5536.
43. Feng, S.; Yang, Y.; Li, M.; Wang, J.; Cheng, Z.; Li, J.; Ji, G.; Yin, G.; Song, F.; Wang, Z.; Li, J.; Gao, X., High-Performance Perovskite Solar Cells Engineered by an Ammonia Modified Graphene Oxide Interfacial Layer. *ACS Applied Materials & Interfaces* **2016,** *8* (23), 14503-14512.
44. Bao, Q.; Braun, S.; Wang, C.; Liu, X.; Fahlman, M., Interfaces of (Ultra) thin Polymer Films in Organic Electronics. *Advanced Materials Interfaces* **2018**, 1800897.
45. Li, Y.; Xu, Z.; Zhao, S.; Qiao, B.; Huang, D.; Zhao, L.; Zhao, J.; Wang, P.; Zhu, Y.; Li, X., Highly Efficient p-i-n Perovskite Solar Cells Utilizing Novel Low-Temperature Solution-Processed Hole Transport Materials with Linear π-Conjugated Structure. *Small* **2016,** *12* (35), 4902-4908.
46. Lim, K. G.; Kim, H. B.; Jeong, J.; Kim, H.; Kim, J. Y.; Lee, T. W., Boosting the power conversion efficiency of perovskite solar cells using self-organized polymeric hole extraction layers with high work function. *Advanced materials* **2014,** *26* (37), 6461-6466.

47. Zhang, H.; Wang, H.; Chen, W.; Jen, A. K. Y., CuGaO2: A Promising Inorganic Hole-Transporting Material for Highly Efficient and Stable Perovskite Solar Cells. *Advanced Materials* **2017,** *29* (8), 1604984.
48. Cho, H.; Jeong, S.-H.; Park, M.-H.; Kim, Y.-H.; Wolf, C.; Lee, C.-L.; Heo, J. H.; Sadhanala, A.; Myoung, N.; Yoo, S., Overcoming the electroluminescence efficiency limitations of perovskite light-emitting diodes. *Science* **2015,** *350* (6265), 1222-1225.
49. Kim, G. W.; Kang, G.; Choi, K.; Choi, H.; Park, T., Solution Processable Inorganic–Organic Double-Layered Hole Transport Layer for Highly Stable Planar Perovskite Solar Cells. *Advanced Energy Materials* **2018,** *8* (26), 1801386.
50. Zhang, W.; Pathak, S.; Sakai, N.; Stergiopoulos, T.; Nayak, P. K.; Noel, N. K.; Haghighirad, A. A.; Burlakov, V. M.; Sadhanala, A.; Li, W., Enhanced optoelectronic quality of perovskite thin films with hypophosphorous acid for planar heterojunction solar cells. *Nature communications* **2015,** *6*, 10030.
51. Fan, B.; Ying, L.; Zhu, P.; Pan, F.; Liu, F.; Chen, J.; Huang, F.; Cao, Y., All-Polymer Solar Cells Based on a Conjugated Polymer Containing Siloxane-Functionalized Side Chains with Efficiency over 10%. *Advanced Materials* **2017,** *29* (47), 1703906.
52. Xing, G.; Mathews, N.; Sun, S.; Lim, S. S.; Lam, Y. M.; Grätzel, M.; Mhaisalkar, S.; Sum, T. C., Long-range balanced electron-and hole-transport lengths in organic-inorganic CH3NH3PbI3. *Science* **2013,** *342* (6156), 344-347.
53. Yu, W.; Li, F.; Wang, H.; Alarousu, E.; Chen, Y.; Lin, B.; Wang, L.; Hedhili, M. N.; Li, Y.; Wu, K., Ultrathin Cu 2 O as an efficient inorganic hole transporting material for perovskite solar cells. *Nanoscale* **2016,** *8* (11), 6173-6179.
54. Stranks, S. D.; Eperon, G. E.; Grancini, G.; Menelaou, C.; Alcocer, M. J.; Leijtens, T.; Herz, L. M.; Petrozza, A.; Snaith, H. J., Electron-hole diffusion lengths exceeding 1 micrometer in an organometal trihalide perovskite absorber. *Science* **2013,** *342* (6156), 341-344.
55. Cao, Y.; Dou, J.-H.; Zhao, N.-j.; Zhang, S.; Zheng, Y.-Q.; Zhang, J.-P.; Wang, J.-Y.; Pei, J.; Wang, Y., Highly efficient NIR-II photothermal conversion based on an organic conjugated polymer. *Chemistry of Materials* **2016,** *29* (2), 718-725.
56. Kim, H.-S.; Mora-Sero, I.; Gonzalez-Pedro, V.; Fabregat-Santiago, F.; Juarez-Perez, E. J.; Park, N.-G.; Bisquert, J., Mechanism of carrier accumulation in perovskite thin-absorber solar cells. *Nature communications* **2013,** *4*, 2242.
57. Dualeh, A.; Moehl, T.; Tétreault, N.; Teuscher, J.; Gao, P.; Nazeeruddin, M. K.; Grätzel, M., Impedance spectroscopic analysis of lead iodide perovskite-sensitized solid-state solar cells. *ACS nano* **2013,** *8* (1), 362-373.
58. Xu, X.; Zhang, H.; Cao, K.; Cui, J.; Lu, J.; Zeng, X.; Shen, Y.; Wang, M., Lead Methylammonium Triiodide Perovskite-Based Solar Cells: An Interfacial Charge-Transfer Investigation. *ChemSusChem* **2014,** *7* (11), 3088-3094.
59. Yang, D.; Yang, R.; Zhang, J.; Yang, Z.; Liu, S. F.; Li, C., High efficiency flexible perovskite solar cells using superior low temperature TiO 2. *Energy & Environmental Science* **2015,** *8* (11), 3208-3214.
60. Sin, D. H.; Ko, H.; Jo, S. B.; Kim, M.; Bae, G. Y.; Cho, K., Decoupling charge transfer and transport at polymeric hole transport layer in perovskite solar cells. *ACS applied materials & interfaces* **2016,** *8* (10), 6546-6553.
61. Xiao, Y.; Han, G.; Chang, Y.; Zhou, H.; Li, M.; Li, Y., An all-solid-state perovskite-sensitized solar cell based on the dual function polyaniline as the sensitizer and p-type hole-transporting material. *Journal of Power Sources* **2014,** *267*, 1-8.
62. Chen, K.; Hu, Q.; Liu, T.; Zhao, L.; Luo, D.; Wu, J.; Zhang, Y.; Zhang, W.; Liu, F.; Russell, T. P., Charge-carrier balance for highly efficient inverted planar heterojunction perovskite solar cells. *Advanced Materials* **2016,** *28* (48), 10718-10724.
63. Fabregat-Santiago, F.; Garcia-Belmonte, G.; Mora-Seró, I.; Bisquert, J., Characterization of nanostructured hybrid and organic solar cells by impedance spectroscopy. *Physical Chemistry Chemical Physics* **2011,** *13* (20), 9083-9118.
64. Pockett, A.; Eperon, G. E.; Peltola, T.; Snaith, H. J.; Walker, A.; Peter, L. M.; Cameron, P. J., Characterization of planar lead halide perovskite solar cells by impedance spectroscopy, open-circuit

photovoltage decay, and intensity-modulated photovoltage/photocurrent spectroscopy. *The Journal of Physical Chemistry C* **2015,** *119* (7), 3456-3465.
65. Jiang, X.; Wang, D.; Yu, Z.; Ma, W.; Li, H. B.; Yang, X.; Liu, F.; Hagfeldt, A.; Sun, L., Molecular Engineering of Copper Phthalocyanines: A Strategy in Developing Dopant-Free Hole-Transporting Materials for Efficient and Ambient-Stable Perovskite Solar Cells. *Advanced Energy Materials* **2019,** *9* (4), 1803287.

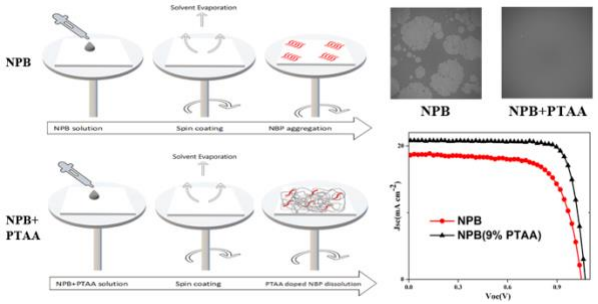

Polymeric dopant strategy distinctly suppressed molecular aggregations and surface dewetting of NPB small molecule hole transport layer in perovskite photovoltaics.